Materials Advances

ROYAL SOCIETY OF CHEMISTRY

PAPER

View Article Online
View Journal | View Issue

Cite this: *Mater. Adv.*, 2026, 7, 484

Elastic properties of diverse sodium-ion conductive materials: a first-principles study

Masato Torii, Atsushi Sakuda,* Kota Motohashi and Akitoshi Hayashi

Received 16th August 2025,
Accepted 4th November 2025

DOI: 10.1039/d5ma00912j

rsc.li/materials-advances

All-solid-state sodium batteries are expected to be low-cost energy-storage devices because they use resource-rich sodium. However, mechanical degradation remains a critical issue, and solid electrolytes must exhibit sufficient ductility to accommodate the expansion and contraction of the electrode active materials at their interface. In this study, the elastic properties of various sodium-ion conductors were evaluated using first-principles calculations and compared based on their anion elements, compositions, crystal phases, and other factors. The elastic moduli of approximately 40 sodium-ion conductors were calculated. The results revealed that sulfide-, chloride-, and hydride-based materials generally exhibit low elastic moduli, whereas oxide materials exhibit higher values. Among the evaluated sulfide compounds, β-Na_3PS_4 crystals exhibit a relatively high Pugh's ratio, suggesting sufficient ductility to resist mechanical degradation. Furthermore, $Na_{2.875}Sb_{0.875}W_{0.125}S_4$ exhibited lower elastic moduli and higher Poisson's and Pugh's ratios than Na_3SbS_4. Unsupervised clustering of the bulk and shear moduli identified two distinct categories of oxide electrolytes: those with medium elastic moduli and those with large elastic moduli. Notably, $NaAl_{11}O_{17}$ exhibited the highest elastic modulus and Pugh's ratio among all the ox electrolytes, which was attributed to its high oxide ion concentration. A nonlinear correlation was observed between the elastic moduli and the mean atomic volume across most materials; however, hydrides deviated from this trend, exhibiting low elastic moduli despite their small mean atomic volumes.

Introduction

Driven by the global transition to renewable energy, the demand for sustainable energy storage devices has increased significantly in recent years. Among the various types of energy storage devices, all-solid-state sodium batteries (ASSBs) are expected to be promising alternatives to conventional lithium-ion batteries owing to their safety, high energy densities, and the abundance of sodium resources.[1–3] The use of solid electrolytes instead of liquid organic electrolytes offers ASSBs various advantages, including improved safety and high thermal stability. In addition, they enable the use of sodium metal as a negative electrode, which leads to high energy densities. However, several issues remain regarding the development of high-performance ASSBs. Mechanical degradation at the solid–solid interface between the electrode active materials and solid electrolytes is caused by the expansion and contraction of the electrode active material during charging and discharging. These volumetric changes induce cracks and voids inside the electrode active materials and solid electrolytes.[4] To prevent mechanical degradation, solid electrolytes must have sufficient deformability and ductility to withstand the expansion and contraction of the electrode active materials.

The elastic modulus is a fundamental property that quantifies the resistance of a material to deformation under microscopic elastic strain. During elastic deformation, the stress and strain are proportional, with the elastic modulus serving as a proportionality constant. Solid electrolytes with lower elastic moduli deform more readily under stress, facilitating better interfacial contact with active electrode materials and accommodating volumetric changes during cycling.

The elastic properties are described by various proportionality constants that depend on the plane and direction of the stress and strain. These constants are organized into a four-dimensional elastic tensor, which is often simplified to a two-dimensional form for easier interpretation and computation. The Voigt–Reuss–Hill approximation is widely used to estimate elastic moduli from the tensor components.[5–7] The principal elastic moduli used to evaluate crystalline materials include the polycrystalline Young's modulus (E), bulk modulus (B), and shear modulus (G). Uniaxial Young's modulus represents the proportionality between stress and strain in the uniaxial direction, whereas the polycrystalline Young's modulus (E) provides an average value for polycrystalline materials. B quantifies the

Department of Applied Chemistry, Graduate School of Engineering, Osaka Metropolitan University, 1-1 Gakuen-cho, Naka-ku, Sakai, Osaka 599-8531, Japan. E-mail: saku@omu.ac.jp; Fax: +81-72-2549910; Tel: +81-72-2549331

relationship between isotropic stress and volumetric strain, whereas G describes the angular displacement under an equilibrium shear force. Another parameter essential for mechanical characterization is Poisson's ratio (ν), which represents the ratio of transverse strain to axial strain under uniaxial stress.

Pugh's ratio, defined as the ratio of the bulk modulus to the shear modulus (B/G),[8] is a critical metric for evaluating the mechanical ductility of solid electrolytes.[9] Initially proposed by Pugh for polycrystalline metals, this criterion assesses the tendency of a material for plastic deformation, which occurs when the material is strained beyond its elastic limit. Pugh suggested that materials with $B/G > 1.75$ are more likely to exhibit plastic deformation.[8] However, while this standard is well-established for metals, its applicability to ceramic materials, such as those used in solid electrolytes, remains unverified.

Deng *et al.*[10] performed comprehensive first-principles calculations of the elastic moduli for representative solid electrolytes, including principal sodium-ion conductors. Their work provided a solid foundation for understanding the mechanical properties of these materials. Building on this important groundwork, the present study aims to extend the scope of the investigation to include recently developed sodium-ion conductive solid electrolytes, thereby deepening the insight into their elastic behavior and potential applications.

Sodium-ion-conductive solid electrolytes have been extensively studied, mainly in oxide and sulfide materials. β″-alumina[11] and NASICON,[12,13] discovered in the 1970s, are well-known oxide electrolytes with high ionic conductivity. Sulfide electrolytes are promising due to their higher ionic conductivity and mechanical ductility than those of oxide electrolytes.[14] Furthermore, sulfide electrolytes exhibit greater formability, and they can achieve densification simply by pressing at room temperature.[15] Na_3PS_4 glass-ceramic electrolytes with high sodium-ion conductivity have enabled the development of ASSBs operable at room temperature.[16,17] Various Na_2S–M_xS_y (M: the central group 13, 14, or 15 cations) sulfide electrolytes have been reported, such as Na_5AlS_4 and Na_4SnS_4.[18–28] Na_3SbS_4 is considered especially promising because it combines high ionic conductivity ($>10^{-3}$ S cm^{-1}) with improved air stability, exhibiting minimal hydrogen sulfide (H_2S) evolution.[26–28] Furthermore, $Na_{2.88}Sb_{0.88}W_{0.12}S_4$ electrolytes, which are tungsten-substituted structures of Na_3SbS_4, exhibit ionic conductivity exceeding 10^{-2} S cm^{-1}.[29–31] In addition to oxides and sulfides, various electrolytes incorporating other anionic elements—such as selenides, halides, and hydrides—have been reported. Selenides with compositions similar to those of sulfides, such as Na_3PSe_4 and Na_3SbSe_4.[32,33] Promising chloride sodium-ion conductors, such as Na_3MCl_6 (M = Y or Er), Na_2ZrCl_6, and $NaTaCl_6$, have recently been explored.[34–38] Borohydride electrolytes are also promising materials,[39–43] for example, the ionic conductivity of $Na_2(CB_9H_{10})(CB_{11}H_{12})$ is higher than 7×10^{-2} S cm^{-1}.[44]

In this study, the elastic properties of various sodium-ion conducting solid electrolytes are evaluated using first-principles calculations. Materials were also compared based on factors such as anion elements, compositions, and crystal phases. Furthermore, the elastic moduli of the tungsten-substituted structures of Na_3SbS_4 ($Na_{3-x}Sb_{1-x}W_xS_4$, x = 0.0625 and 0.125) were calculated to investigate the effect of the substitution on their mechanical properties. In addition, the distribution of the elastic moduli of sodium-ion conductive solid electrolytes is analyzed using unsupervised clustering. Correlations between the mean atomic volume (MAV) and elastic moduli are also examined, providing insights into the structural factors that directly determine the elastic properties.

Computational details

The elastic properties of crystal structures were obtained using first-principles calculations based on density functional theory (DFT).[45,46] All first-principles calculations were implemented using the Vienna ab initio simulation package (VASP)[47,48] with the generalized gradient approximation exchange correlation functional in the scheme of Perdew–Burke–Ernzerhof (PBE).[49,50] The projected augmented-wave (PAW) method[51,52] was adopted to describe the pseudopotential of inner-shell electrons. The cut-off energies for the plane wave basis set and electric energy convergence were set at 500 and 10^{-6} eV, respectively. The Monkhorst–Pack scheme[53] was adopted to determine the k-point distributions and irreducible Brillouin zones. Both the lattice constants and ionic positions of the ordinary crystal structures were fully relaxed, and the final forces on all the relaxed atoms were less than 0.01 eV Å^{-1}. The on-site Coulomb term (U) values of 2.50, 3.50, and 4.00 eV for Ti-3d, Zr-4d, and Nb-4d, respectively, were set based on previous studies.[54–57] Spin polarization was not considered in these calculations. The DFT-D3 method with Becke–Johnson damping was adopted to incorporate the van der Waals dispersion energy in the first-principles calculations.[58] MAV was defined as the ratio of the cell volume and the total number of atoms.[10] Note that this cell volume was calculated from lattice constants after structural optimization.

The elastic properties were calculated through the following procedure. The original crystal structures were obtained from the Materials Project[59] and Inorganic Crystal Structure Database (ICSD).[60] Exceptionally, the Na_2ZrCl_6 crystal structure was generated using the supercell program[61] based on the CIF obtained from ICSD, since the Na sites are randomly occupied and a specific configuration needed to be selected from possible candidates. The atomic geometries of crystal structures were then fully optimized using first-principles calculations. Subsequently, the elastic tensors were evaluated for the optimized structures, and the elastic properties of the polycrystalline phase were derived using the Voigt–Reuss–Hill approximation.

The following is an outline of the Voigt–Reuss–Hill approximation method.[5–7] The bulk modulus (B) and shear modulus (G) were obtained as the average values (the Hill's prediction values) of those calculated using Voigt's (B_V and G_V) and Reuss's (B_R and G_R) prediction methods (eqn (1)–(6)). In these equations, each component of the inverse elasticity tensor is represented by S_{ij}. The polycrystalline Young's modulus (E)

and Poisson's ratio (ν) were estimated using eqn (7) and (8), respectively.

$$9B_V = (C_{11} + C_{22} + C_{33}) + 2(C_{12} + C_{23} + C_{31}) \quad (1)$$

$$1/B_R = (S_{11} + S_{22} + S_{33}) + 2(S_{12} + S_{23} + S_{31}) \quad (2)$$

$$B = (B_V + B_R)/2 \quad (3)$$

$$15G_V = (C_{11} + C_{22} + C_{33}) - (C_{12} + C_{23} + C_{31}) + 3(C_{44} + C_{55} + C_{66}) \quad (4)$$

$$15/G_R = 4(S_{11} + S_{22} + S_{33}) - 4(S_{12} + S_{23} + S_{31}) + 3(S_{44} + S_{55} + S_{66}) \quad (5)$$

$$G = (G_V + G_R)/2 \quad (6)$$

$$E = 9BG/(3B + G) \quad (7)$$

$$\nu = (3B - 2G)/2(3B + G) \quad (8)$$

The universal anisotropy (A^U) was calculated using eqn (9).[62,63] If the crystal structure is completely isotropic,

Table 1 First-principles calculation results for the elastic properties on the crystal structures of diverse sodium-ion conductors, which were obtained from both this study and previous studies. These data include the reported data of their ambient ionic conductivities

Type	Formula	Crystal system	B /GPa	G /GPa	E /GPa	ν	B/G	MAV cm^{-3} mol^{-1}	A^U	Ref.	Experimental ionic conductivity/ S cm^{-1} (25–30 °C)
Sulfide	α-Na_3PS_4	Tetragonal	29.85	13.17	34.44	0.308	2.27	12.20	0.72	This study	$>10^{-6}$ (ref. 16)
Sulfide	α-Na_3PS_4	Tetragonal	25.3	13.1	33.6	0.28	2.29	—	0.22	10	
Sulfide	β-Na_3PS_4	Cubic	30.38	9.86	26.68	0.354	3.08	12.13	2.27	This study	4.6×10^{-4} (glass-ceramic)[16,17]
Sulfide	β-Na_3PS_4	Cubic	21.5	13.1	32.6	0.25	1.64	—	0.25	10	
Sulfide	$NaPS_3$	Monoclinic	20.15	7.72	20.55	0.33	2.61	13.3	2.55	This study	—
Sulfide	Na_3SbS_4	Cubic	26.06	11.85	30.87	0.303	2.20	13.28	0.5	This study	$1.0–3.0 \times 10^{-3}$ (ref. 26–28)
Sulfide	Na_3BS_3	Monoclinic	26.43	17.43	42.87	0.23	1.52	11.74	0.28	This study	1.1×10^{-5} (glass)[18]
Sulfide	Na_5AlS_4	Orthorhombic	30.06	14.07	36.52	0.298	2.14	13.23	0.1	This study	3.2×10^{-7} (ref. 19)
Sulfide	Na_3InS_3	Monoclinic	27.23	11.35	29.89	0.317	2.40	14.64	0.92	This study	6.8×10^{-6} (glass)[21]
Sulfide	Na_4SnS_4	Tetragonal	30.59	12.41	32.79	0.321	2.47	13.74	0.96	This study	1.4×10^{-8} (ref. 24)
Sulfide	Na_3AsS_4	Tetragonal	28.91	12.49	32.76	0.311	2.31	12.61	0.55	This study	3.1×10^{-6} (ref. 25)
Selenide	Na_3PSe_4	Cubic	27.44	10.34	27.56	0.333	2.65	13.95	0.32	This study	1.1×10^{-4} (ref. 32)
Selenide	Na_3PSe_4	Cubic	20	9	23	0.31	2.22	—	0.34	67	
Selenide	Na_3SbSe_4	Cubic	24.76	9.18	24.51	0.335	2.70	15.04	0.13	This study	8.5×10^{-4} (ref. 33)
Anti-perovskite	Na_3OBr	Cubic	35.09	25.8	62.16	0.205	1.36	11.11	0.11	This study	—
Anti-perovskite	Na_3OBr	Cubic	34	23.6	57.4	0.22	1.44	—	0.14	10	
Anti-perovskite	Na_3OCl	Cubic	35.48	25.98	62.65	0.206	1.37	10.66	0.32	This study	—
Anti-perovskite	Na_3OCl	Cubic	36.4	24.6	60.2	0.22	1.48	—	0.20	10	
Anti-perovskite	$Na_3OBr_{0.5}Cl_{0.5}$	Cubic	35.18	25.64	61.88	0.207	1.37	10.88	0.2	This study	—
NASICON	$NaZr_2(PO_4)_3$	Trigonal	88.42	46.82	119.39	0.275	1.89	8.76	0.32	This study	8.9×10^{-6} (ref. 68)
NASICON	$NaZr_2(PO_4)_3$	Trigonal	86.3	47.7	120.9	0.27	1.81	—	0.41	10	
NASICON	$NaZr_2(PO_4)_3$	Trigonal	93	46	118	0.29	2.02	—	0.33	67	
NASICON	$NaTi_2(PO_4)_3$	Trigonal	115.22	57.55	148.01	0.286	2.00	7.79	0.25	This study	$10^{-4}–1.1 \times 10^{-3}$ (ref. 69)
NASICON	$NaTi_2(PO_4)_3$	Trigonal	109	56	144	0.28	1.95	—	0.24	67	
NASICON	$Na_3Sc_2(PO_4)_3$	Trigonal	64.79	43.11	105.85	0.228	1.50	7.89	3.01	This study	3×10^{-4} (ref. 70)
NASICON	$Na_3Sc_2(PO_4)_3$	Monoclinic	89.15	46.58	119.01	0.277	1.91	7.92	0.51	This study	—
NASICON	$Na_4Zr_2(SiO_4)_3$	Trigonal	98.16	56.45	142.11	0.259	1.74	7.89	0.36	This study	—
NASICON	$Na_4Zr_2(SiO_4)_3$	Trigonal	93	57	141	0.25	1.63	—	0.37	67	
NASICON	$Na_3Zr_2Si_2PO_{12}$	Triclinic	98.33	48.8	125.63	0.287	2.01	8.34	0.63	This study	6.7×10^{-4} (ref. 71)
NASICON	$Na_3Zr_2Si_2PO_{12}$	Monoclinic	78.73	50.5	124.81	0.236	1.56	8.16	0.63	This study	—
NASICON	$Na_3Hf_2Si_2PO_{12}$	Monoclinic	90.59	55.42	138.10	0.246	1.63	7.96	0.58	This study	1.48×10^{-3} (ref. 72)
Na-β-alumina	$NaAl_{11}O_{17}$	Hexagonal	153.94	62.76	165.75	0.321	2.45	6.42	2.11	This study	—
Other oxide	$NaAlO_2$	Orthorhombic	86.27	45.36	115.78	0.276	1.90	7.44	0.68	This study	—
Other oxide	Na_5AlO_4	Orthorhombic	59.85	33.79	85.31	0.262	1.77	7.91	0.05	This study	—
Other oxide	Na_5AlO_4	Orthorhombic	51	30	74	0.26	1.70	—	0.06	67	
Other oxide	$Na_7Al_3O_8$	Triclinic	68.28	39.53	99.40	0.257	1.73	7.68	0.31	This study	—
Other oxide	$Na_7Al_3O_8$	Triclinic	68	46	111	0.25	1.48	—	0.52	67	
Other oxide	$Na_{14}Al_4O_{13}$	Monoclinic	66.60	37.38	94.48	0.264	1.78	8.04	0.06	This study	—
Other oxide	$Na_{17}Al_5O_{16}$	Monoclinic	67.30	37.74	95.39	0.264	1.78	7.99	0.05	This study	—
Other oxide	$Na_{17}Al_5O_{16}$	Monoclinic	58	34	86	0.25	1.71	—	0.12	67	
Other oxide	Na_3BO_3	Monoclinic	58.58	27.47	71.28	0.297	2.13	7.19	0.66	This study	2.0×10^{-8} (glass)[73]
Other oxide	Na_3BO_3	Monoclinic	52	25	64	0.29	2.08	—	0.67	67	
Other oxide	Na_4SiO_4	Triclinic	67.41	36.47	92.70	0.271	1.85	7.61	0.3	This study	—
Other oxide	Na_4SiO_4	Triclinic	58	32	81	0.27	1.81	—	0.43	67	
Other oxide	Na_3SbO_4	Monoclinic	80.34	52.08	128.47	0.233	1.54	7.34	0.37	This study	—
Other oxide	Na_3SbO_4	Monoclinic	67	44	108	0.23	1.52	—	0.87	67	
Other oxide	Na_3NbO_4	Monoclinic	79.04	51.59	127.12	0.232	1.53	7.32	0.28	This study	—
Other oxide	Na_3NbO_4	Monoclinic	69	42	104	0.25	1.64	—	0.62	67	
Chloride	$NaAlCl_4$	Orthorhombic	13.72	6.88	17.68	0.285	2.00	15.09	0.17	This study	3.9×10^{-6} (ref. 74)
Chloride	$NaAlCl_4$	Orthorhombic	5	3	7	0.26	1.67	—	3.92	67	
Chloride	$NaTaCl_6$	Monoclinic	11.67	5.97	15.31	0.281	1.95	15.44	0.72	This study	6.2×10^{-5} (ref. 38)
Chloride	Na_2ZrCl_6	Trigonal	18.67	8.28	21.65	0.307	2.25	15.49	0.29	This study	1.8×10^{-5} (ref. 35)
Chloride	Na_3ErCl_6	Monoclinic	24.71	11.37	29.57	0.301	2.17	14.58	0.42	This study	—

$A^U = 0$: the farther the A^U deviates from 0, the higher the degree of anisotropy.

$$A^U = 5\frac{G_V}{G_R} + \frac{B_V}{B_R} - 6 \quad (9)$$

These elastic properties were extracted from the elastic tensors using VASPKIT.[64] Unsupervised clustering was performed using the *k*-means algorithm implemented in the scikit-learn library[65] in Python 3.10. To examine the effect of elemental substitution, the atomic charges of the $Na_{3-x}Sb_{1-x}W_xS_4$ crystal structures were calculated using the Bader analysis.[66]

Results and discussion

The calculated elastic moduli for various crystal structures of the sodium-ion conductors and reported experimental ambient ionic conductivities are summarized in Table 1. This table includes the first-principles calculation data of previous studies.[10,67] Before the discussion, the experimentally obtained elastic moduli of previously reported Na-ion conductors were summarized. Representative crystal structures are shown in Fig. 1. Previous data on the elastic moduli of Na_2S–P_2S_5 glass sulfide electrolytes experimentally obtained by the ultrasonic method are summarized in Table S1.[75] It is important to note that the calculations in this study represent theoretical predictions based on crystal morphology. Consequently, the mechanical properties of the corresponding powder compacts should be investigated independently to validate these findings. There is a valuable previous study for the experimental elastic moduli of NASICON electrolytes based on $Na_3Zr_2Si_2PO_{12}$,[76] although they contain several impurities and the relative densities of the samples are not close to 100%. The Young's modulus of β-alumina has been experimentally determined using the

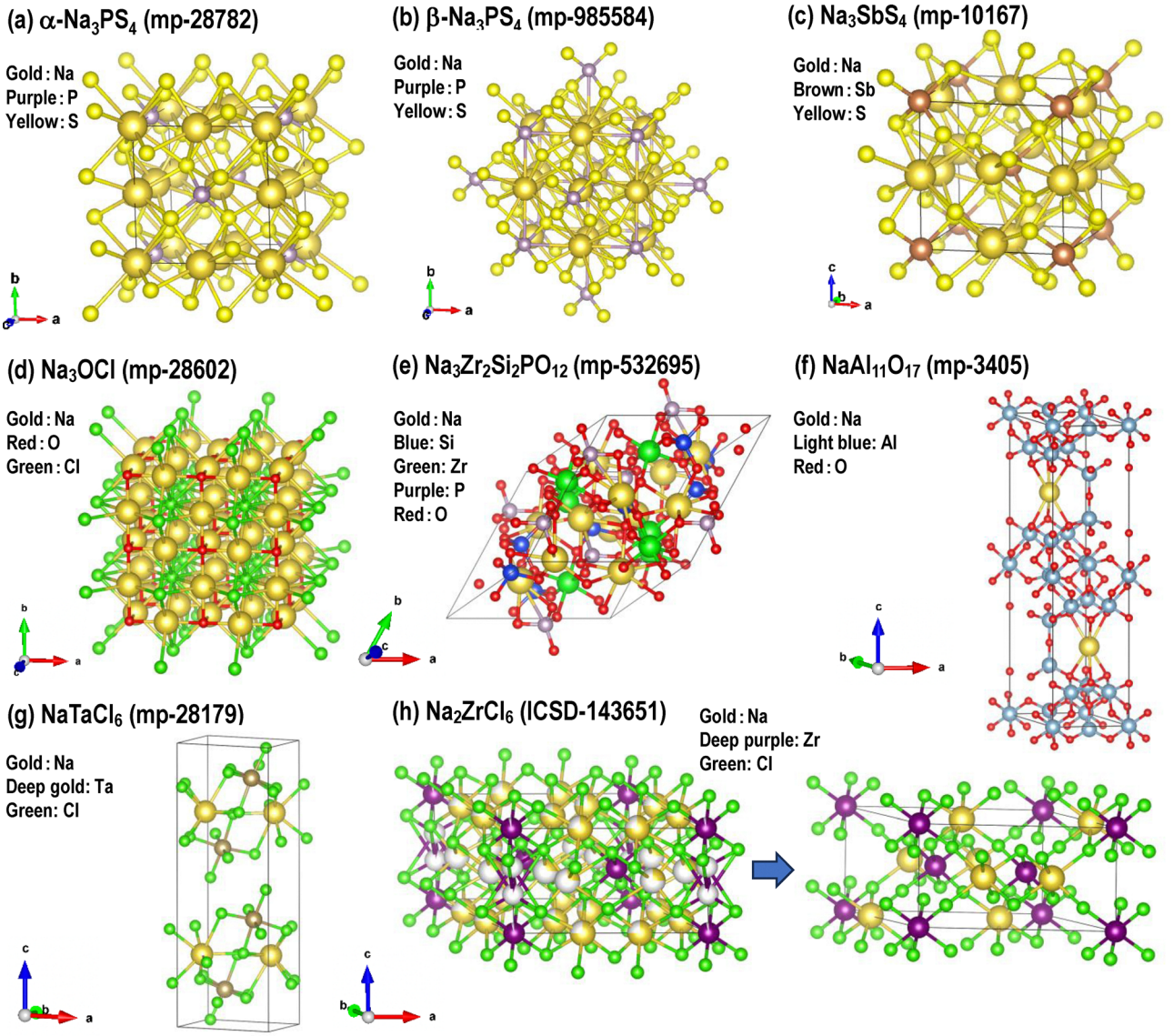

Fig. 1 Various typical crystal structures which have been used as sodium-ion conductors.

hardness indentation method, yielding two different values, 215 and 174 GPa, depending on the plane of indentation.[77]

Generally, sulfides, selenides, and chlorides tend to have lower elastic moduli, whereas oxides tend to have higher elastic moduli. The overall order of the elastic moduli follows the trend: oxides > sulfides > selenides > chlorides. The general trend observed for Pugh's ratio (B/G) is selenides > sulfides > chlorides > oxides. Many sodium-ion conductors, except for some sulfides and oxides, exceed the ductility/brittleness criterion for polycrystalline metals (B/G = 1.75), suggesting that they are ductile electrolytes at the crystal structure scale. The A^U values were below 1 for most systems, except for a few cases such as β-Na_3PS_4 and $NaPS_3$, suggesting that the elastic properties of most sodium-ion conductors are isotropic.

Sulfides are characterized by relatively low elastic moduli, and many materials exhibit relatively high B/G values. Among the polymorphs of Na_3PS_4, the high-temperature phase, β-Na_3PS_4, has significantly lower G and E than the low-temperature phase, α-Na_3PS_4. Notably, β-Na_3PS_4 has an exceptionally high B/G ratio of 3.08, whereas all other materials listed in Table 1 exhibit B/G values below 3. This suggests that β-Na_3PS_4 possesses particularly higher mechanical ductility. Notably, $NaPS_3$ exhibits relatively low elastic moduli. In addition, Na_3BS_3 displays a remarkably low B/G ratio of 1.4, indicating low ductility. This behavior contrasts with the general trend observed for sulfides. Selenides generally exhibit slightly lower elastic moduli and higher B/G ratios than sulfides. The elastic moduli of the glassy $NaPS_3$ electrolyte tended to be lower than those of the crystalline Na_3PS_4. It was predicted that this tendency is due to the larger MAV of the glassy phase, resulting in weaker chemical bonding compared to the crystalline phase. In contrast, the Poisson's and Pugh's ratios of $NaPS_3$ were almost the same for both glassy and crystalline phases. The Poisson's and Pugh's ratios of glassy $NaPS_3$ were intermediate between those of β- and α-Na_3PS_4, relatively closer to those of the β-phase.

The elastic moduli of the oxide electrolytes can generally be classified into two groups, high and moderate, except for anti-perovskite electrolytes that exhibit lower elastic moduli and $NaAl_{11}O_{17}$ with extremely high elastic moduli. The elastic moduli of the oxides largely depend on their oxygen content. Materials with an oxygen content exceeding 50% tend to be classified as "high," and those with a lower oxygen content as "moderate." These two classifications are discussed again in the section that presents the unsupervised clustering results. The Pugh's ratios (B/G) of most oxides ranged from 1.5 to 2.0. The distinctive mechanical properties of $NaAl_{11}O_{17}$ include not only significant elastic moduli but also a relatively high B/G ratio of 2.45. Materials with high elastic moduli generally exhibit low Pugh's ratios, making this property unique. This suggests that $NaAl_{11}O_{17}$ is not only an exceptionally rigid material but also has the potential to possess ductility.

The chloride electrolytes generally exhibit lower elastic moduli than the sulfide and selenide electrolytes, indicating their high deformability. Their Pugh's ratios (B/G) were approximately 2.0, which is relatively low compared to sulfides but exceeds the threshold value of 1.75 exhibit the lowest elastic moduli and a B/G ratio of 1.95, indicating that it is a

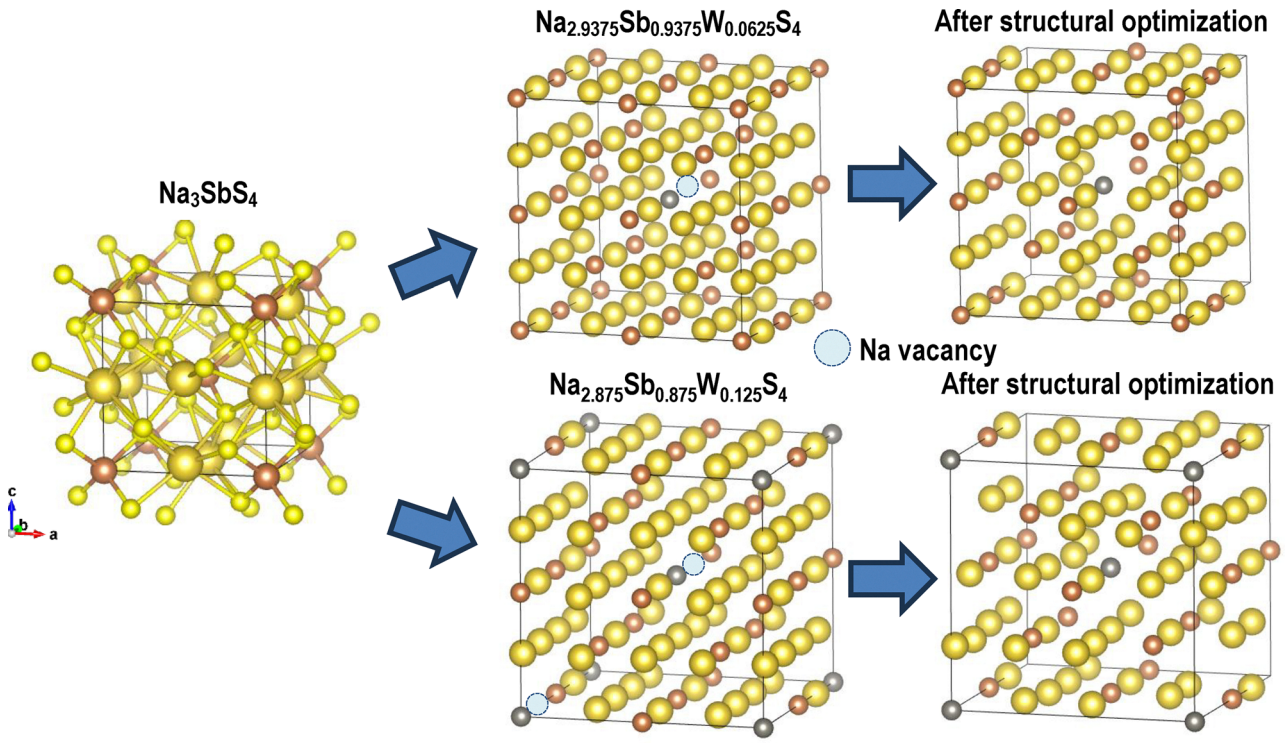

Fig. 2 Flowchart on creating $Na_{3-x}Sb_{1-x}W_xS_4$ crystal model structures by substituting Sb atom with W atom and doping Na vacancies. In the substituted structures, the anion atoms are omitted from visualization.

useful electrolyte with sufficient mechanical deformability and ductility.

To predict the elastic properties of $Na_{2.88}Sb_{0.88}W_{0.12}S_4$, a sodium-ion conductor with exceptionally high ionic conductivity, we calculated the elastic moduli of analogous structures derived by partially substituting tungsten into Na_3SbS_4.

The crystal structure model of Na_3SbS_4 (six Na, two Sb, and eight S atoms) was obtained from the Materials Project database. The structure was expanded into a 2 × 2 × 2 supercell (48 Na, 16 Sb, and 64 S atoms) using the VASPKIT software. In these supercells, tungsten substitution was implemented as shown in Fig. 2. For $Na_{2.9375}Sb_{0.0625}W_{0.0625}S_4$, a single Sb atom at the center of the cell was replaced with W, and for $Na_{2.875}Sb_{0.875}W_{0.125}S_4$, the Sb atoms at both the center and corners of the cell were replaced with W atoms. In addition, it was assumed that the Na atoms in the vicinity of the W atoms would be removed because of their proximity. For $Na_{2.875}Sb_{0.875}W_{0.125}S_4$, both the Na atoms adjacent to the W atoms were removed. After structural optimization, the elastic moduli of all the compositions were calculated, as summarized in Table 2.

Despite the negligible change in MAV owing to tungsten substitution, the bulk modulus increased significantly, whereas the shear modulus and polycrystalline Young's modulus decreased slightly. Consequently, the B/G ratio increased, indicating a transition to a more ductile material. Before the tungsten substitution, the B/G ratio was 2.20, which increased to 2.78 and 3.57 for $Na_{2.9375}Sb_{0.0625}W_{0.0625}S_4$ and $Na_{2.875}Sb_{0.875}W_{0.125}S_4$, respectively. For the composition $Na_{2.875}Sb_{0.875}W_{0.125}S_4$, the B/G ratio was higher than that of β-Na_3PS_4 (3.08), which was the highest among the materials listed in Table 1. These results suggest that tungsten substitution significantly enhances the ductility of Na_3SbS_4, making it one of the most ductile sodium-ion conductors. The Poisson's ratio of $Na_{2.875}Sb_{0.875}W_{0.125}S_4$ was also higher than that of Na_3SbS_4, further indicating that the crystal structure was more prone to deformation under the applied stress.

Table 2 Calculated elastic moduli of various model crystal structures of $Na_{3-x}Sb_{1-x}W_xS_4$

Formula	B/GPa	G/GPa	E/GPa	ν	B/G	MAV/cm^3 mol^{-1}	A^U
Na_3SbS_4	26.06	11.85	30.87	0.303	2.20	13.28	0.50
$Na_{2.9375}Sb_{0.9375}W_{0.0625}S_4$	30.54	10.97	29.39	0.34	2.78	13.35	0.49
$Na_{2.875}Sb_{0.875}W_{0.125}S_4$	38.26	10.72	29.41	0.372	3.57	13.41	0.43

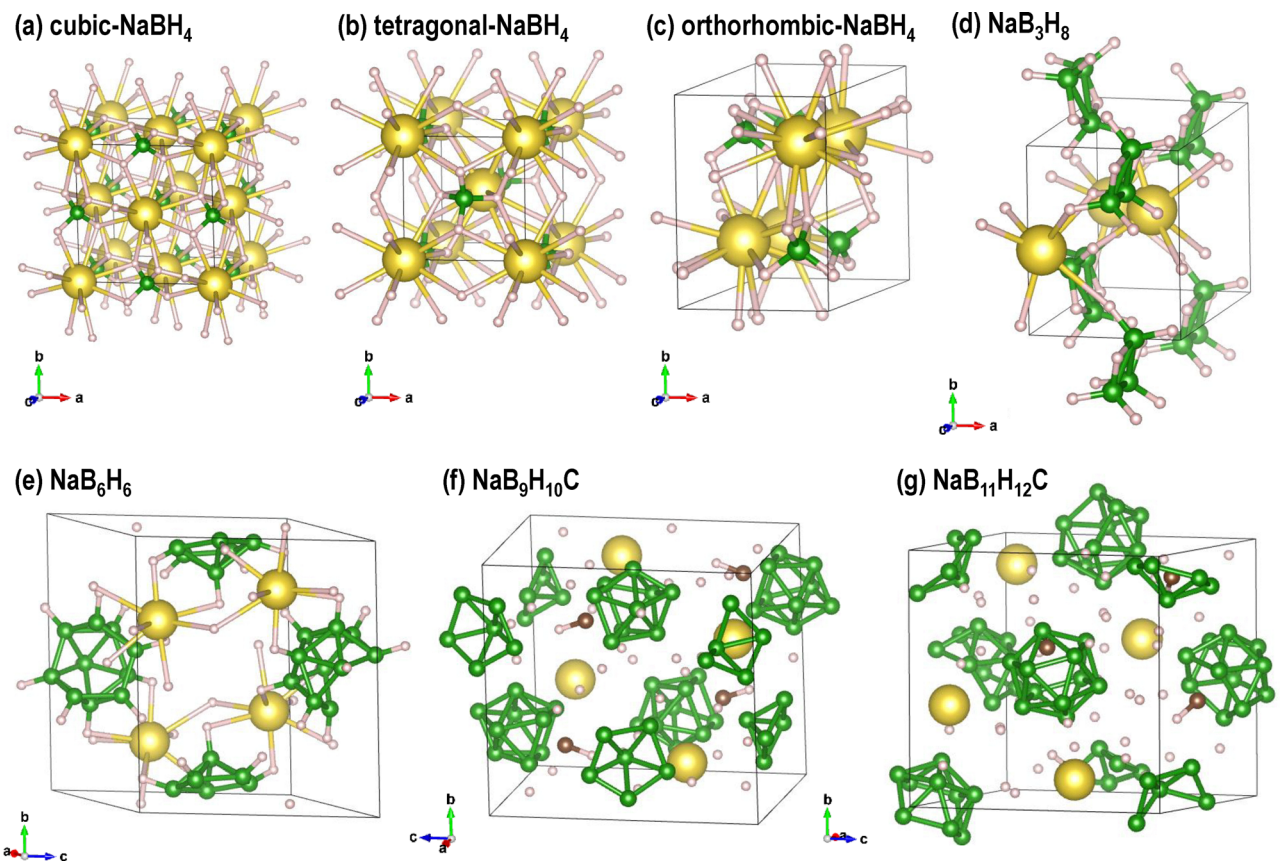

Fig. 3 Unit cell structures of various sodium-ion conductors with boron hydrides; gold: sodium, green: boron, pink: hydrogen.

The results of Bader charge analysis are shown in Table S2. The positive charge on W (+1.63) is greater than that on Sb (approximately +1.45). This indicates a stronger Coulombic interaction between the central cation and surrounding sulfur atoms, which is considered to be the cause of the higher bulk modulus. Furthermore, this enhancement of the Coulombic interaction is suggested to have no significant effect on the shear modulus and polycrystalline Young's modulus.

Fig. 3 shows the structures of the various borohydride-based sodium solid electrolytes employed in this study. Because of the presence of multiple crystal phases of $NaBH_4$, three different structures were prepared. The structure of $NaBH_4$ consists of Na^+ ions coordinated to BH_4^- tetrahedra. NaB_3H_8 features a structure in which Na^+ ions are coordinated to $B_3H_8^-$ units, which can be described as clusters. Similarly, NaB_6H_6, $NaB_9H_{10}C$, and $NaB_{11}H_{12}C$ exhibit structures in which the Na^+ ions are coordinated around clusters containing multiple B atoms.

The calculated elastic moduli of the borohydride-based sodium-ion conductors are summarized in Table 3. Despite having exceptionally low MAVs, these materials exhibit elastic moduli comparable to those of sulfide-based solid electrolytes. This behavior is unique compared to that of other sodium solid electrolytes. Notably, the shear modulus of $NaB_{11}H_{12}C$ is as low as 6.92 GPa. The B/G ratio, which varies depending on the material and crystal system, had relatively high values, exceeding 2.0 for NaB_6H_6 and $NaB_{11}H_{12}C$. In contrast, $NaB_9H_{10}C$ exhibited a relatively low B/G ratio, comparable to those of the oxide electrolytes. The A^U exceeded 1 in certain systems, but remained low overall. These findings suggest that the borohydride-based solid electrolytes exhibit elastic isotropy.

The calculated elastic moduli of the Na_xY-type and Na_3PO_4 crystals are summarized in Table S3. Compared with lithium-based materials, the elastic moduli of these sodium-based compounds are generally lower, with Na_2Se and NaI exhibiting particularly low values. However, many of these materials have relatively low B/G ratios, falling below the threshold value of 1.75. Na_3PO_4 exhibited moderate elastic moduli compared to other sodium-ion conductors with a B/G ratio of 1.98, which is not particularly low.

Fig. 4 shows the distribution of the bulk and shear moduli of the sodium-ion conductors investigated in this study. Fig. 4a illustrates the distribution of materials with relatively low elastic moduli (primarily non-oxide materials), while Fig. 4b displays the distribution of oxides, excluding those with an anti-perovskite structure, which generally exhibit higher elastic

Table 3 Calculated elastic moduli of crystal structures of various borohydride-based sodium-ion conductors

Type	Formula	Crystal system	B/GPa	G/GPa	E/GPa	ν	B/G	MAV/cm^3 mol^{-1}	A^U	Ref.	Experimental ionic conductivity/S cm^{-1} (25–30 °C)
Hydride	$NaBH_4$	Cubic	22.53	17.21	41.15	0.195	1.31	5.31	0.02	This study	$\cong 10^{-10}$ [78]
Hydride	$NaBH_4$	Tetragonal	25.88	14.54	36.74	0.263	1.78	5.13	0.43	This study	—
Hydride	$NaBH_4$	Orthorhombic	22.57	14.97	36.77	0.228	1.51	5.15	0.06	This study	—
Hydride	NaB_3H_8	Orthorhombic	19.21	11.00	27.71	0.26	1.75	4.76	0.31	This study	—
Hydride	NaB_6H_6	Monoclinic	20.21	8.68	22.78	0.312	2.33	5.58	1.49	This study	$\cong 10^{-8}$ [79]
Hydride	NaB_6H_6	Monoclinic	10	6	15	0.27	1.67	—	1.59	67	
Hydride	$NaB_9H_{10}C$	Orthorhombic	18.21	9.98	25.32	0.268	1.82	5.52	0.5	This study	0.03 [80]
Hydride	$NaB_{11}H_{12}C$	Orthorhombic	16.32	6.92	18.2	0.314	2.36	5.21	1.43	This study	$\cong 10^{-5}$ [81]

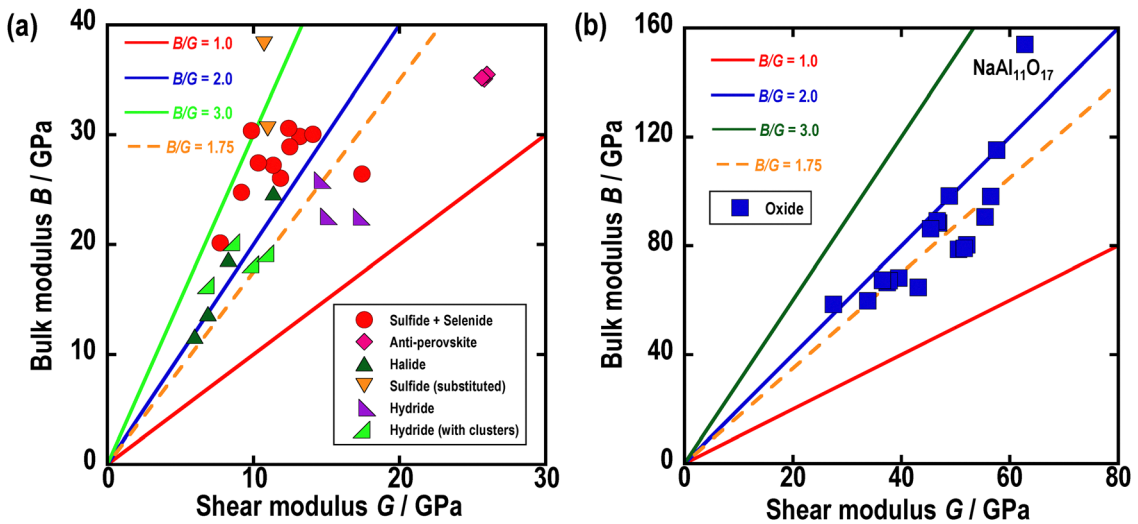

Fig. 4 Correlation between bulk Modulus (B) and shear Modulus (G) of various sodium-ion conductors: (a) electrolytes with lower elastic moduli: sulfides, selenides, anti-perovskite electrolytes, halides, and hydrides, (b) electrolytes with higher elastic moduli: oxides except for anti-perovskite electrolytes.

moduli. As shown in Fig. 4a, many materials exhibit B/G ratios that exceed the threshold value of 1.75. In contrast, the $NaBH_4$, Na_3BS_3, and anti-perovskite structures have B/G ratios well below 1.75. Notably, only two materials, β-Na_3PS_4 and $Na_{2.875}Sb_{0.875}W_{0.125}S_4$, exhibit B/G ratios exceeding 3. As shown in Fig. 4b, most oxide electrolytes were distributed at approximately B/G = 1.75. However, $NaAl_{11}O_{17}$ is an exceptional case with a significantly high B/G ratio.

The results of the unsupervised clustering using the k-means method (k = 4) based on the bulk and shear moduli are shown in Fig. 5. Materials can be primarily divided into four classes: those with low, medium, and high elastic moduli and materials with exceptionally high elastic moduli. The low-elastic moduli region (cluster 0) consists of sulfides, selenides, halides (excluding fluorides), hydrides, and anti-perovskite-type electrolytes. Oxides (and fluorides) are mainly divided into those with medium elastic moduli (cluster 2) and those with high elastic moduli (cluster 1). $NaTi_2(PO_4)_3$ and $NaAl_{11}O_{17}$, exhibiting exceptionally high elastic moduli, were classified into a group of materials with extremely high elastic moduli (cluster 3).

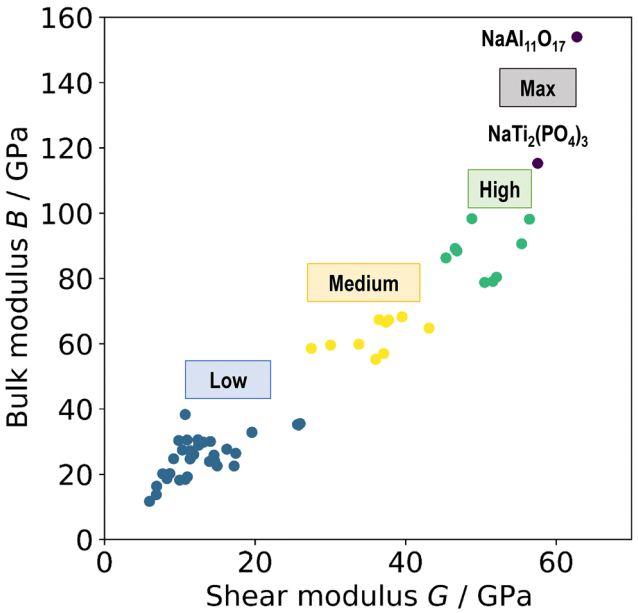

Fig. 5 Clustering of sodium-ion conductors based on bulk modulus (B) and shear modulus (G) using k-means method with four clusters.

Fig. 6 shows the correlations between MAV and elastic properties (a: bulk modulus, b: polycrystalline Young's modulus, and c: shear modulus). A negative nonlinear correlation exists between MAV and each elastic modulus when the hydrides are excluded. However, focusing on the oxide electrolytes reveals that even with similar MAV values, the elastic moduli can differ significantly. This result confirms that factors other than MAV, such as the space group and crystal system, influence the elastic properties. Among the oxides, anti-perovskite structures, which contain halogens, tend to exhibit higher MAV and lower elastic moduli. Sulfides display a negative correlation between the MAV and elastic moduli, with the correlation being particularly pronounced for the bulk and shear moduli. By contrast, chlorides exhibit exceptionally high MAV values and notably low elastic moduli. Hydrides are exceptional because they exhibit low MAVs and low elastic moduli.

A comparative analysis was also conducted with Li-ion-conducting solid electrolytes. The computational results obtained for the Na-ion-conducting solid electrolytes in this study were generally similar to those for Li-ion-conducting solid electrolytes obtained from first-principles calculations.[82] A slight difference was observed in the bulk modulus of sulfide electrolytes: while many Li-ion conductive solid electrolytes exhibited values around 30–40 GPa, most Na-based ones showed lower values of approximately 20–30 GPa. Consequently, materials with B/G ratios clearly exceeding 3.0, which are often found in Li-ion conductive solid electrolytes, were much less common in the Na-ion conductive solid electrolytes. Furthermore, experimental measurements of the elastic moduli of sulfide glass electrolytes revealed a correlation between the average atomic volume and Young's modulus.[9] This correlation is consistent with the one observed for the Na-ion-conducting solid electrolytes in this study, and a

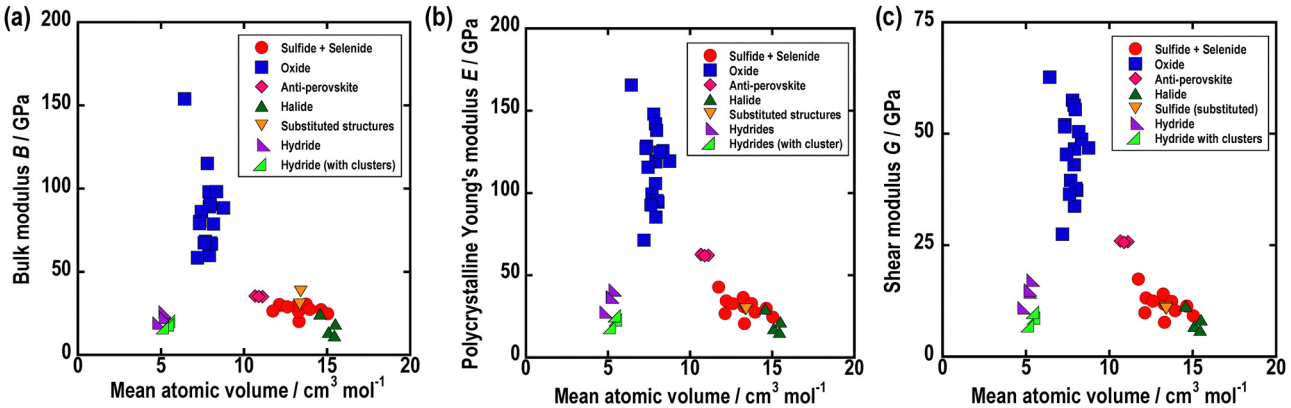

Fig. 6 Correlation between mean atomic volume and (a) bulk moduli B, (b) polycrystalline elastic moduli E, and (c) shear moduli G of various crystal structures of various sodium-ion conductors.

similar trend has also been reported in the computational results for Li-ion conductive solid electrolytes.[82]

As a reference data for the comparison, elastic moduli extracted from Materials Project were listed in Table S4. Although there are slight differences in the values due to variations in computational conditions, such as lattice constants, the elastic properties are generally consistent with those obtained in this study and in previous calculations. This study also includes the elastic moduli of many electrolytes that are not available in the Materials Project or previous reports, making it a valuable contribution in this respect.

Conclusions

In this study, the elastic properties and Pugh's ratios (B/G) of various sodium-ion conductive solid electrolytes were estimated using first-principles calculations. Sulfides, chlorides, and hydrides generally exhibited low elastic moduli, with β-Na_3PS_4 showing a notably high Pugh's ratio, suggesting high ductility. Oxide electrolytes were categorized as materials with medium-to-high elastic moduli, with a clear trend of higher elastic moduli correlated with an increased oxygen content. Among oxides, $NaAl_{11}O_{17}$ was identified as having the highest elastic modulus and Pugh's ratio, indicating unique mechanical properties, as materials with high elastic moduli typically show lower Pugh's ratios.

The substitution of tungsten into Na_3SbS_4 resulted in significant changes not only in ionic conductivity but also in elastic properties. Specifically, the bulk modulus and Poisson's ratio increased, whereas the polycrystalline Young's and shear moduli decreased. This resulted in an increase in Pugh's ratio, suggesting enhanced mechanical ductility. Across the studied materials, those with high ionic conductivities, such as β-Na_3PS_4 and $Na_{2.875}Sb_{0.875}W_{0.125}S_4$, were found to have relatively high Poisson's ratios. A negative nonlinear correlation was observed between the MAV and elastic moduli. Borohydride-based electrolytes deviated from this trend by exhibiting low elastic moduli despite their low MAV.

These findings provide valuable insights into the mechanical properties of sodium-ion conductive solid electrolytes and offer guidance for the design of mechanically stable materials for all-solid-state batteries.

Author contributions

Masato Torii: performed the simulations, processed the results, wrote the manuscript. Atsushi Sakuda: supervised the work, revised the manuscript. Kota Motohashi: provided critical feedback, revised the manuscript. Akitoshi Hayashi: provided critical feedback, revised the manuscript.

Conflicts of interest

There are no conflicts to declare.

Data availability

The database IDs of the solid electrolytes used in this study, the number of k-points, and their lattice constants obtained after structural optimization for the elastic tensor calculations are listed in Table S5. We have compiled the elastic modulus data in CSV format as well as the elastic tensor data on the following GitHub page. **https://github.com/MasatoTorii/Na_ElasticDB**.

Supplementary information (SI) is available. See DOI: **https://doi.org/10.1039/d5ma00912j**.

Acknowledgements

This study was supported by the MEXT/JSPS KAKENHI (grant number JP23H04633), MEXT Program: Data Creation and Utilization-Type Material Research and Development Project (JPMXP1122712807), JST Adopting Sustainable Partnerships for Innovative Research Ecosystem (JPMJAP2313), JST SPRING (grant number JPMJSP2139) and the 2024 Osaka Metropolitan University (OMU) Strategic Research Promotion Project (Priority Research). First-principles calculations were partially performed using the computing resources offered under the category of General Projects by the Research Institute for Information Technology, Kyushu University.

References

1 K. Takada, *Acta Mater.*, 2013, **61**, 759.
2 Y. Kato, S. Hori, T. Saito, K. Suzuki, M. Hirayama, A. Mitsui, M. Yonemura, H. Iba and R. Kanno, *Nat. Energy*, 2016, **1**, 16030.
3 J. Janek and W. G. Zeier, *Nat. Energy*, 2016, **1**, 16141.
4 A. Hayashi, A. Sakuda and M. Tatsumisago, *Front. Energy Res.*, 2016, **4**, 25.
5 W. Voigt, *Lehrbuch Kristallphys.*, 1928.
6 A. Z. Reuss, *Z. Angew. Math. Mech.*, 1929, **9**, 49–58.
7 R. Hill, *Proc. Phys. Soc. A*, 1952, **65**, 349–354.
8 S. F. Pugh, *Philos. Mag.*, 1954, **45**, 823–843.
9 A. Kato, M. Nose, M. Yamamoto, A. Sakuda, A. Hayashi and M. Tatsumisago, *J. Ceram. Soc. Jpn.*, 2018, **126**, 719.
10 Z. Deng, Z. Wang, I. H. Chu, J. Luo and S. P. Ong, *J. Electrochem. Soc.*, 2016, **163**, A67.
11 A. Hooper, *J. Phys. D*, 1977, **10**, 1487.
12 J. B. Goodenough, H. Y.-P. Hong and J. A. Kafalas, *Mater. Res. Bull.*, 1976, **11**, 203.
13 O. Bohnke, S. Ronchetti and D. Mazza, *Solid State Ionics*, 1999, **122**, 127.
14 J. Lau, R. H. DeBlock, D. M. Butts, D. S. Ashby, C. S. Choi and B. S. Dunn, *Adv. Energy Mater.*, 2018, **8**, 1800933.
15 A. Sakuda, A. Hayashi and M. Tatsumisago, *Sci. Rep.*, 2013, **3**, 2261.
16 A. Hayashi, K. Noi, A. Sakuda and M. Tatsumisago, *Nat. Commun.*, 2012, **3**, 856.
17 A. Hayashi, K. Noi, N. Tanibata, M. Nagao and M. Tatsumisago, *J. Power Sources*, 2014, **258**, 420.

18 F. Tsuji, A. Nasu, C. Hotehama, A. Sakuda, M. Tatsumisago and A. Hayashi, *Mater. Adv.*, 2021, **2**, 1676.
19 S. Harm, A. K. Hatz, C. Schneider, C. Hoefer, C. Hoch and B. V. Lotsch, *Front. Chem.*, 2020, **8**, 90.
20 K. Denoue, D. Lecoq, C. Calers, A. Gautier, L. Verger and L. Calvez, *Mater. Res. Bull.*, 2021, **142**, 111423.
21 K. Motohashi, A. Nasu, T. Kimura, C. Hotehama, A. Sakuda, M. Tatsumisago and A. Hayashi, *Electrochemistry*, 2022, **90**, 067009.
22 N. Tanibata, K. Noi, A. Hayashi and M. Tatsumisago, *RSC Adv.*, 2014, **4**, 17120.
23 M. Ribes, B. Barrau and J. L. Souquet, *J. Non-Cryst. Solids*, 1980, **38–39**, 271.
24 L. Gao, G. Bian, Y. Yang, B. Zhang, X. Wu and K. Wu, *New J. Chem.*, 2021, **45**, 12362.
25 Z. Yu, S. L. Shang, J. H. Seo, D. Wang, X. Luo, Q. Huang, S. Chen, J. Lu, X. Li, Z. K. Liu and D. Wang, *Adv. Mater.*, 2017, **29**, 1605561.
26 L. Zhang, D. Zhang, K. Yang, X. Yan, L. Wang, J. Mi, B. Xu and Y. Li, *Adv. Sci.*, 2016, **3**, 1600089.
27 H. Wang, Y. Chen, Z. D. Hood, G. Sahu, A. S. Pandian, J. K. Keum, K. An and C. Liang, *Angew. Chem., Int. Ed.*, 2016, **55**, 8551.
28 A. Banerjee, K. H. Park, J. W. Heo, Y. J. Nam, C. K. Moon, S. M. Oh, S. T. Hong and Y. S. Jung, *Angew. Chem., Int. Ed.*, 2016, **55**, 9634.
29 A. Hayashi, N. Masuzawa, S. Yubuchi, F. Tsuji, C. Hotehama, A. Sakuda and M. Tatsumisago, *Nat. Commun.*, 2019, **10**, 5266.
30 T. Fuchs, S. P. Culver, P. Till and W. G. Zeier, *ACS Energy Lett.*, 2020, **5**, 146.
31 A. Nasu, T. Otono, T. Takayanagi, M. Deguchi, A. Sakuda, M. Tatsumisago and A. Hayashi, *Energy Storage Mater.*, 2024, **67**, 103307.
32 S.-H. Bo, Y. Wang, J. C. Kim, W. D. Richards and G. Ceder, *Chem. Mater.*, 2016, **28**, 252–258.
33 S. Xiong, Z. Liu, H. Rong, H. Wang, M. McDaniel and H. Chen, *Sci. Rep.*, 2018, **8**, 9146.
34 R. Schlem, A. Banik, M. Eckardt, M. Zobel and W. G. Zeier, *ACS Appl. Energy Mater.*, 2020, **3**, 10164–10173.
35 H. Kwak, J. Lyoo, J. Park, Y. Han, R. Asakura, A. Remhof, C. Battaglia, H. Kim, S.-T. Hong and Y. S. Jung, *Energy Storage Mater.*, 2021, **37**, 47–54.
36 Y. Qie, S. Wang, S. Fu, H. Xie, Q. Sun and P. Jena, *J. Phys. Chem. Lett.*, 2020, **11**, 3376–3383.
37 D. Park, K. Kim, G. H. Chun, B. C. Wood, J. H. Shim and S. Yu, *J. Mater. Chem. A*, 2021, **9**, 23037–23045.
38 K. Motohashi, H. Tsukasaki, A. Sakuda, S. Mori and A. Hayashi, *ACS Mater. Lett.*, 2024, **6**, 1178–1183.
39 W. S. Tang, M. Matsuo, H. Wu, V. Stavila, W. Zhou, A. A. Talin, A. V. Soloninin, R. V. Skoryunov, O. A. Babanova, A. V. Skripov, A. Unemoto, S. I. Orimo and T. J. Udovic, *Adv. Energy Mater.*, 2016, **6**, 1502237.
40 W. S. Tang, A. Unemoto, W. Zhou, V. Stavila, M. Matsuo, H. Wu, S. I. Orimo and T. J. Udovic, *Energy Environ. Sci.*, 2015, **8**, 3637–3645.
41 T. J. Udovic, M. Matsuo, W. S. Tang, H. Wu, V. Stavila, A. V. Soloninin, R. V. Skoryunov, O. A. Babanova, A. V. Skripov, J. J. Rush, A. Unemoto, H. Takamura and S. I. Orimo, *Adv. Mater.*, 2014, **26**, 7622–7626.
42 T. J. Udovic, M. Matsuo, A. Unemoto, N. Verdal, V. Stavila, A. V. Skripov, J. J. Rush, H. Takamura and S. Orimo, *Chem. Commun.*, 2014, **50**, 3752.
43 X.-W. Chen, J.-X. Kang, Z.-H. Fan, N. Zhang, W.-Y. Zhang, G.-G. Zhang, A.-Q. Zhu, Z.-W. Lu, P. Qiu, Y. Wu and X. Chen, *Small*, 2024, **20**, 2401439.
44 W. S. Tang, K. Yoshida, A. V. Soloninin, R. V. Skoryunov, O. A. Babanova, A. V. Skripov, M. Dimitrievska, V. Stavila, S. Orimo and T. J. Udovic, *ACS Energy Lett.*, 2016, **1**, 659–664.
45 P. Hohenberg and W. Kohn, *Phys. Rev.*, 1964, **136**, B864.
46 W. Kohn and L. J. Sham, *Phys. Rev.*, 1965, **140**, A1133.
47 G. Kresse and J. Furthmüller, *Phys. Rev. B: Condens. Matter Mater. Phys.*, 1996, **54**, 11169.
48 G. Kresse and J. Furthmüller, *Comput. Mater. Sci.*, 1996, **6**, 15.
49 J. P. Perdew, K. Burke and M. Ernzerhof, *Phys. Rev. Lett.*, 1996, **77**, 3865.
50 J. P. Perdew, K. Burke and M. Ernzerhof, *Phys. Rev. Lett.*, 1997, **78**, 1396.
51 P. E. Blöchl, *Phys. Rev. B: Condens. Matter Mater. Phys.*, 1994, **50**, 17953.
52 G. Kresse and D. Joubert, *Phys. Rev. B: Condens. Matter Mater. Phys.*, 1999, **59**, 1758.
53 H. J. Monkhorst and J. D. Pack, *Phys. Rev. B: Condens. Matter Mater. Phys.*, 1976, **13**, 5188.
54 Z. Hu and H. Metiu, *J. Phys. Chem. C*, 2011, **115**, 5841.
55 X. Lu, S. Wang, R. Xiao, S. Shi, H. Li and L. Chen, *Nano Energy*, 2017, **41**, 626.
56 S. Kc, R. C. Longo, K. Xiong and K. Cho, *Solid State Ionics*, 2014, **261**, 100.
57 H. Kamisaka, T. Suenaga, H. Nakamura and K. Yamashita, *J. Phys. Chem. C*, 2010, **114**, 12777.
58 S. Grimme, S. Ehrlich and L. Goerigk, *J. Comput. Chem.*, 2011, **32**, 1456.
59 A. Jain, S. P. Ong, G. Hautier, W. Chen, W. D. Richards, S. Dacek, S. Cholia, D. Gunter, D. Skinner, G. Ceder and K. A. Persson, *APL Mater.*, 2013, **1**, 011002.
60 G. Bergerhoff, R. Hundt, R. Sievers and I. D. Brown, *J. Chem. Inf. Comput. Sci.*, 1983, **23**, 66.
61 K. Okhotnikov, T. Charpentier and S. Cadars, *J. Cheminform.*, 2016, **8**, 17.
62 S. I. Ranganathan and M. Ostoja-Starzewski, *Phys. Rev. Lett.*, 2008, **101**, 055504.
63 C. M. Kube, *AIP Adv.*, 2016, **6**, 095209.
64 V. Wang, N. Xu, J.-C. Liu, G. Tang and W.-T. Geng, *Comput. Phys. Commun.*, 2021, **267**, 108033.
65 F. Pedregosa, G. Varoquaux, A. Gramfort, V. Michel, B. Thirion, O. Grisel, M. Blondel, P. Prettenhofer, R. Weiss, V. Dubourg, J. Vanderplas, A. Passos, D. Cournapeau, M. Brucher, M. Perrot and É. Duchesnay, *J. Mach. Learn. Res.*, 2011, **12**, 2825.
66 R. F. W. Bader, *Acc. Chem. Res.*, 1985, **18**, 9.

67 K. Min, *J. Electrochem. Soc.*, 2021, **168**, 030541.
68 Y. Ji, T. Honma and T. Komatsu, *Solid State Ionics*, 2023, **395**, 116213.
69 H. Dai, W. Xu, Z. Hu, Y. Chen, J. Gu, F. Xie, W. Wei, R. Guo and G. Zhang, *ACS Omega*, 2021, **6**, 11537.
70 D. Rettenwander, G. J. Redhammer, M. Guin, A. Benisek, H. Krüger, O. Guillon, M. Wilkening, F. Tietz and J. Freig, *Chem. Mater.*, 2018, **30**, 1776.
71 Z. Jian, Y. S. Hu, X. Ji and W. Chen, *Adv. Mater.*, 2017, **29**, 1601925.
72 S. Chai, H. Tian, J. Liu, S. Liu, L. Dai, J. Xu, L. Kong and L. Wang, *J. Mater. Chem. A*, 2022, **10**, 1284.
73 K. Suzuki, Y. Nakamura, N. Tanibata, A. Hayashi and M. Tatsumisago, *J. Asian Ceram. Soc.*, 2016, **4**, 6.
74 M. Häfner and M. Bianchini, *J. Phys. Chem. C*, 2024, **128**, 19978.
75 M. Nose, A. Kato, A. Sakuda, A. Hayashi and M. Tatsumisago, *J. Mater. Chem. A*, 2015, **3**, 22061.
76 E. J. Cheng, T. Yang, Y. Liu, L. Chai, R. G. Mendez, E. Kazyak, Z. Fu, G. Luo, F. Chen, R. Inada, V. Badilita, H. Duan, Z. Wang, J. Qin, H. Li, S. Orimo and H. Kato, *Mater. Today Energy*, 2024, **44**, 101644.
77 D. C. Hitchcock and L. C. E. Jonghe, *J. Asian Ceram. Soc.*, 1983, **66**, c204.
78 X. Luo and K. F. A. Zinsou, *Ionics*, 2020, **26**, 5287.
79 Y. Sadikin, P. Schouwink, M. Brighi, Z. Łodziana and R. Černý, *Inorg. Chem.*, 2017, **56**, 5006.
80 W. S. Tang, M. Matsuo, H. Wu, V. Stavila, W. Zhou, A. A. Talin, A. V. Soloninin, R. V. Skoryunov, O. A. Babanova, A. V. Skripov, A. Unemoto, S. Orimo and T. J. Udovic, *Adv. Energy Mater.*, 2016, **6**, 1.
81 W. S. Tang, A. Unemoto, W. Zhou, V. Stavila, M. Matsuo, H. Wu, V. Stavila, S. Orimo and T. J. Udovic, *Energy Environ. Sci.*, 2015, **8**, 3637.
82 M. Torii, A. Sakuda, K. Motohashi and A. Hayashi, *Mater. Adv.*, 2025, **6**, 6445.